Published in final edited form as:
Conf Proc IEEE Eng Med Biol Soc. 2011 August ; 2011: 5977–5980. doi:10.1109/IEMBS.2011.6091477.

Dynamic Phase Imaging for in Vitro Process Monitoring and Cell Tracking

Katherine Creath[Member, EMBS, IEEE]
K. Creath is with 4D Technology Corporation, Tucson, AZ 85706 USA, College of Optical Sciences, The University of Arizona, Tucson, AZ 85720 USA, and Optineering, Tucson, AZ 85719 USA. (kcreath@ieee.org).

Abstract

This paper describes a new, novel quantitative interference microscope system and presents images, videos and data of live biological samples. The specially designed optical system enables instantaneous 4-dimensional video measurements of dynamic motions within and among live cells without the need for contrast agents. This “label-free”, vibration insensitive imaging system enables measurement of biological objects in reflection using harmless light levels with a variety of magnifications and wavelengths with fields of view from several hundred microns up to a millimeter. At the core of the instrument is a phase measurement camera (PMC) enabling simultaneous measurement of multiple interference patterns utilizing a pixelated phase mask taking advantage of the polarization properties of light. Phase values are converted to optical thickness data enabling volumetric, motion and morphological studies. Data from organisms such as flagellates and rotifers will be presented, as will measurements of human breast cancer cells with the addition of various agents that break down the cells. These data highlight examples of monitoring different biological processes and cellular motions.

I. Introduction

THE ability to instantaneously measure live cells, and follow motions and processes over time, provides valuable information to researchers studying cellular dynamics, motility, and cell and tissue morphology. Quantitative phase imaging can measure structures from interference images analogous to those viewed with phase-contrast imaging and differential interference contrast imaging. Phase images can reveal features and quantitative data that are not available through conventional imaging. Phase imaging measures optical thickness variations due to small variations in refractive index relating to variations in density of different structures and materials within cells and tissues. Very small refractive index variations can manifest as large variations in phase images. Phase image data enable quantitative measurements that aren’t possible with standard microscopy techniques. Samples do not need to be stained, labeled or marked, and harmless light levels are used. By taking short snapshots in radid succession, the dimension of time opens up the ability to track motions of cells, see how cells interact with one another, and follow small motions within cells, tissues and structures. This type of imaging with quantitative analysis enables new types of studies involving cell tracking and process monitoring.

II. Background

Full-field phase-imaging interference microscopes have been around since the early 1980’s [1-3]. High precision measurements on small surfaces have been obtained for engineering surfaces such as hard disk substrates, magnetic heads for hard drives, and critical dimension measurement for lithography [3]. Techniques developed for these instruments have relied upon phase-measurement methods, which predominantly obtain interferograms sequentially,

and therefore require good vibrational damping, and static specimens so that high-quality data can be obtained. Most interferometric microscopes have utilized narrowband illumination with short coherence lengths of tens of microns. The reason for narrowband "low coherence" illumination is to reduce effects of reflections off of nearby surfaces and to help reduce effects of speckle in the imaging systems. With biological samples, low coherence illumination enables the samples to be isolated in space without getting spurious interference patterns from other surfaces (mainly the coverslip). These techniques have been used for biological measurements but have not been utilized as much as they could because they are predominantly sensitive to motion and vibration [4-10].

As an alternative, pixelated phase mask sensor technology uniquely provides a single frame phase measurement in a compact, robust format that is compatible with conventional microscope imagining systems, and permits the use of a wide variety of wavelengths and source bandwidths [11-13]. It enables the creation of a versatile and compact microscope interferometer for biological applications. These sensors have been implemented in many different types of interferometers and are insensitive to vibration and do not require scanning. All necessary information to determine phase is recorded in a single snapshot [11-13].

A. Linnik Interference Microscope

The interference microscope used for this work is based upon a Linnik configuration [3]. It is comprised of a Köhler-type illumination system utilizing a low coherence extended source [14], and a simple imaging system as shown in Fig. 1. An aperture stop enables controlling the size of the source in the entrance pupil of the microscope objectives, while a field stop enables easier alignment of the system.

This particular design utilizes polarized light so that the object and reference beams have orthogonal polarizations. The incoming illumination is split into orthogonal polarizations before the microscope objective using a polarization beamsplitter. The relative irradiances of the test and object beam are balanced for maximum contrast using the polarizer. A quarter-wave plate (QWP) before the camera combines the two polarized beams so that the two beams can interfere at the pixelated phase mask. The extended source reduces coherent noise, spurious reflections, and enables isolation of a small depth region within the sample. For the measurements in this paper, samples in water or cell media are viewed in reflection through a cover slip.

Source wavelengths can vary throughout the visible and near infrared, while a variety of objective magnifications can be utilized. For the examples presented in this paper, sources with wavelengths of 785 nm and 660 nm were used with 10X NA 0.3 and 20X NA 0.5 objectives. The imaging "tube" lens magnification was either 1X or 1.67X.

B. Phase Determination with Pixelated Phase Mask

Fig. 2 illustrates how the micropolarizers are spatially distributed and oriented in a pixelated polarization mask. When the reference and test beams are combined, each having orthogonal circular polarization (right-hand circular and left-hand circular), the measured intensity at each pixel of the mask is given by

$$I(x,y)=\frac{1}{2}\left\{I_r+I_s+2\sqrt{I_r I_s}\cos\left[\Delta\varphi(x,y)+2\alpha_p\right]\right\},$$

where α_p is the angle of the polarizer with respect to the *x, y* plane, I_r and I_s are the irradiances of reference and signal beams respectively, and $\Delta\phi(x,y)$ is the optical path

difference between the beams. Using this equation we obtain different phase shifts for each type of pixel: A (0°), B (90°), C (180°) and D (270°). A single interferogram image uses all pixels of one type (e.g. A). Brightfield images are obtained by averaging all 4 types of pixels. Optical thickness (OT) is obtained by solving the 4 pixel types for $\Delta\phi(x,y)$ with λ as the wavelength. One solution is given by

$$OT = \left(\frac{\lambda}{4\pi}\right)\Delta\varphi(x,y) = \left(\frac{\lambda}{4\pi}\right) ATAN\left\{\frac{C(x,y) - A(x,y)}{D(x,y) - B(x,y)}\right\}$$ [15, 16]. These calculations can be performed in real time. Bright field, phase contrast, and optical thickness can be simultaneously obtained dynamically.

C. Measuring Optical Thickness

This type of microscope directly measures phase, specifically the phase difference between the reference beam and the test beam, also known as optical path difference (OPD). Each interference fringe in reflection corresponds to one-half wave of OPD. Typically, the raw units of this measure are in terms of wavelengths of the source light (waves).

To make these data more useful we convert the phase data to optical thickness *OT(x,y)* which is given by

$$OT(x,y) = OPD \cdot \frac{\lambda}{2} = \phi(x,y)\left[\frac{\lambda}{4\pi}\right]$$

Optical thickness (*OT*) is an integrated measure of the overall optical path through the sample, which is the product of the localized index of refraction *n(x,y,z)* and the physical thickness *t(x,y,z)*,

$$OT(x,y) = \int_o^T n(x,y,z) \cdot t(x,y,z)\, dz$$

For viewing in reflection measurements these examples yield OT in double pass through the coverslip and liquid containing the objects. Denser areas of the object with higher indices of refraction will yield a larger *OT* as shown in Fig. 3. Typically, the index of refraction of the coverslip is ~1.5, the index of water is ~1.33, while cellular media is ~1.37, cytoplasm ~1.39 and cellular organelles like nuclei ~1.41-1.43. Subtle differences as small as the third decimal place in refractive index are detectable by this system.

III. Dynamic Phase Images

A. Flagellate – Cell Tracking

Flagellates utilize flagella for mobility to help them sense and move. Fig. 4 shows a sequence of images of a flagellate. The organism is spinning and the flagellum is moving significantly between frames. These are samples from a 3.5 s movie with 3 ms exposures. Motion between images is similar to what it looks like with a time scale of 0.1 s intervals. The flagellum is about 5 μm in diameter and about 80-100 μm long. The pseudocolor scale has been set with limits that bring out the flagellum while clipping the maximum (red) and minimum (blue) optical thickness values of the body and organelles.

B. Breast Cancer Cell Culture – Process Monitoring

Cell cultures of the MCF715 human breast cancer line were grown in cell media on coverslips. To image these cells, the coverslips were placed upside down on a highly reflective mirror with cell media filling in between the mirror and coverslip. These images

were taken at 20X with a 1.67X tube lens, a 660 nm source and 2 ms exposures. Cell cultures can also be measured directly on glass slides with media and a coverslip, but for the same short exposure times this would require a more powerful source.

Fig. 5 shows an image of some of these cells. Note that the intercellular matrix and newly forming cells around the edges of the matrix are clearly visible and easily resolved as are organelles and nuclei within the cells. The lateral sampling in the image for this exposure is 0.53 μm for each 4-pixel 2×2 cell in the pixelated phase mask. The optical resolution at NA=0.5 is 0.8 μm (0.61 λ/NA) yielding a slightly oversampled image. To process this image so that different optical thickness layers have different colors, the background shape due to the mirror and coverslip has been subtracted out by fitting piston, tilt, curvature and cylinder (basically removing a best fit 2^{nd}-order polynomial surface) from the areas where there are not cells present [17].

Fig. 6 shows the cells of Fig. 5 after contact with purified water and then a KCL solution. There is noticeable osmotic swelling of the cells while the structure around the outer edges has shriveled. Notice that hardly anything is visible in brightfield, while the interference image shows definite detail that is brought out in the quantitative phase images.

Fig. 7 shows some images of another cell culture of human breast cancer cells after contact with various media. All of these images are scaled in optical thickness to the same limits of −100 to 450 nm so that changes are more obvious. In Fig. 7(A) the cells are in their growth media. In Fig. 7(B) the cells have been exposed to purified water causing them to osmotically swell. Fig. 7(C) shows how they further swell and flatten after further exposure to purified water while Fig. 7(D) shows the cells after then being exposed to NaOH. For each of these cases, 4D phase movies were recorded showing changes every few seconds. Changes are obvious as seen in these few images.

After this series of images, the cells were then exposed to Alconox® (a detergent containing enzymes). Once the cells have osmotically swelled from purified water and begun breaking down by NaOH, the Alconox® further breaks down the cell walls and the cells dissolve. Fig. 8 shows a series of images from a longer 4D phase movie taken as the cells were dissolving. The movie images were taken every 4 seconds over a 78 second time span while Fig. 8 shows snapshots every 10 seconds. With more time resolution it is possible to watch how the cells break down and dissolve.

IV. Discussion and Conclusion

This paper has shown a number of examples of 4D phase measurements of living biological organisms and how they may be tracked dynamically as they move or as perturbations are made to their environment. The short exposure times freeze motion instantaneously and since all data to determine phase and optical thickness can be gathered in a single snapshot, no scanning is necessary. Harmless light levels along with no need for staining, labeling or marking cells offers a non-destructive means of observing and quantifying biological behavior and dynamic variations over time. The ability to dynamically measure biological organisms in real time opens up many different types of applications ranging from flow cytometry to tissue dynamics, morphological and volumetric studies along with mechanistic studies, process monitoring, quantification of cellular motion, monitoring and tracking cellular damage under known perturbations, tracking cell migration, nerve and muscle transmission, histology and photodynamic therapy. This model can also be extended to higher magnifications, immersion objectives, higher numerical apertures, a large range of wavelengths, and viewing cells in transmission as well as reflection. Data from brightfield imaging and phase contrast (interference image) are also obtained simultaneously along with

phase and optical thickness. Conceptually, this model could be further modified to include simultaneous fluorescence measurements to more specifically track particular mechanisms.

Acknowledgments

Thanks to my collaborators: James Millerd and Neal Brock of 4D Technology Corp., Andrew Rouse and Arthur Gmitro from The University of Arizona Dept. of Radiology, and Adam Wax of Duke University.

This work was supported in part by NIH/NCRR: 1 R43 RR028170-01 and 2 R44 RR028170-02.

REFERENCES

[1]. Sommargren GE. Optical Heterodyne Profilometry. Applied Optics. 1981; vol. 20:610–618. [PubMed: 20309165]

[2]. Wyant JC, et al. An optical profilometer for surface characterization of magnetic media. ASLE Trans. 1984; vol. 27:101–113.

[3]. Schmit, J., et al. Chapter 15: Surface Profiling, Multiple Wavelength and White Light Interferometry. In: Malacara, D., editor. Optical Shop Testing. 3rd Edition. Wiley; New York: 2007. p. 667-755.

[4]. Dunn GA, Zicha D. Phase-Shifting Interference Microscopy Applied to the Analysis of Cell Behaviour. Symposia of the Society for Experimental Biology. 1993; vol. 47:91–106. [PubMed: 8165581]

[5]. Tychinsky VP, et al. Quantitative real-time analysis of nucleolar stress by coherent phase microscopy. J Biomedical Optica. 2008; vol. 13:064032.

[6]. Yang C, et al. Phase-referenced interferometer with subwavelength and subhertz sensitivity applied to the study of cell membrane dynamics. Optics Letters. Aug.2001 vol. 26:1271–1273. [PubMed: 18049583]

[7]. Popescu, G. Quantitative Phase Imaging of Nanoscale Cell Structure and Dynamics. In: Jena, BP., editor. Methods in Nano Cell Biology. Vol. vol. 90. Elsevier; San Diego: 2008. p. 87-115.Volume 90

[8]. Hogenboom DO, et al. Three-dimensional images generated by quadrature interferometry. Optics Letters. May.1998 vol. 23:783–785. [PubMed: 18087341]

[9]. Reed J, et al. High throughput cell nanomechanics with mechanical imaging interferometry. Nanotechnology. Jun.2008 vol. 19

[10]. Yu LF, et al. Quantitative phase evaluation of dynamic changes on cell membrane during laser microsurgery. Journal of Biomedical Optics. Sep-Oct.2008 vol. 13

[11]. Brock, NJ., et al. Pixelated phase-mask interferometer. United States Patent. 7,230,717. June 12. 2007 2007

[12]. Kimbrough BT. Pixelated mask spatial carrier phase shifting interferometry algorithms and associated errors. Applied Optics. Jul.2006 vol. 45:4554–4562. [PubMed: 16799664]

[13]. Novak M, et al. Analysis of a micropolarizer array-based simultaneous phase-shifting interferometer. Applied Optics. 2005; vol. 44:6861–6868. [PubMed: 16294959]

[14]. Born, M.; Wolf, E. Principles of Optics. 5th ed. Pergamon Press; Oxford: 1975.

[15]. Creath, K. Phase-measurement interferometry techniques. In: Wolf, E., editor. Progress in Optics. Vol. vol. 26. Elsevier Science Publishers; Amsterdam: 1988. p. 349-393.

[16]. Creath, K.; Schmit, J. Phase measurement interferometry. In: Guenther, RD., et al., editors. Encyclopedia of Modern Optics. Elsevier; 2004. p. 364-374.

[17]. Malacara, D., et al. Interferogram analysis for optical testing. 2nd ed. Taylor & Francis; Boca Raton, FL: 2005.

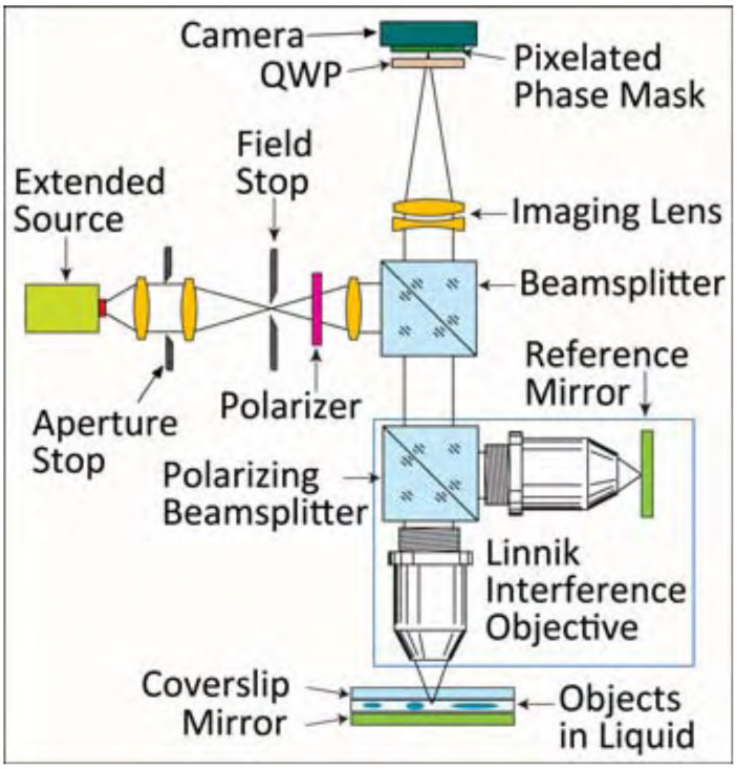

Fig. 1.
Optical schematic of Linnik interference microscope.

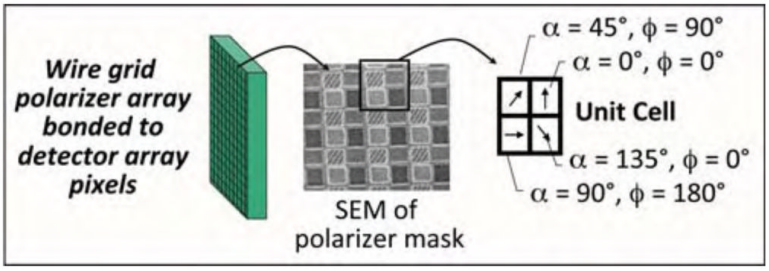

Fig. 2.
Pixelated phase mask sensor is an array of wire grid micropolarizers on a glass substrate bonded to the detector array. The phase mask is comprised of 4 different polarizations comprising a unit cell of 2×2 different phase shifts as noted above.

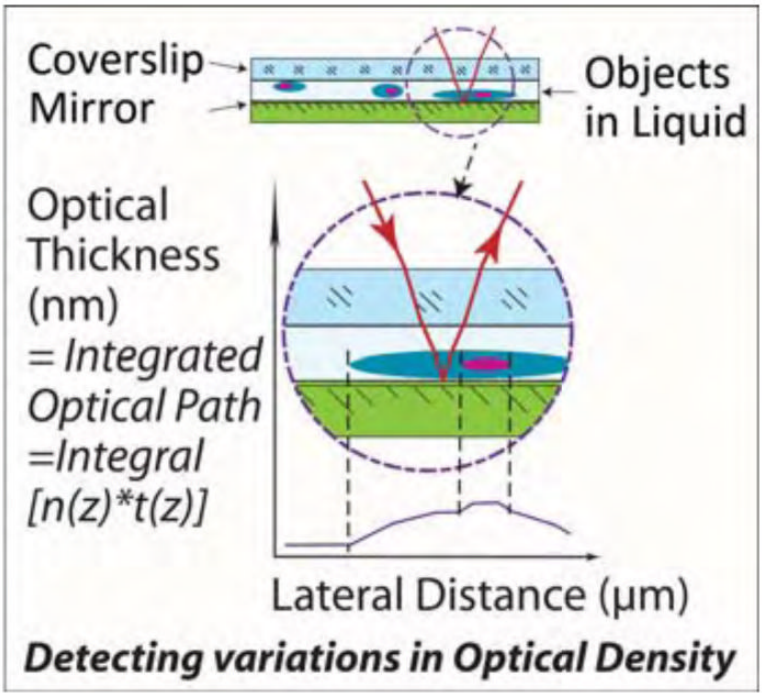

Fig. 3.
Path length through test sample including coverslip, liquid and objects. Graph (bottom) shows optical thickness profile for the section within the highlighted area.

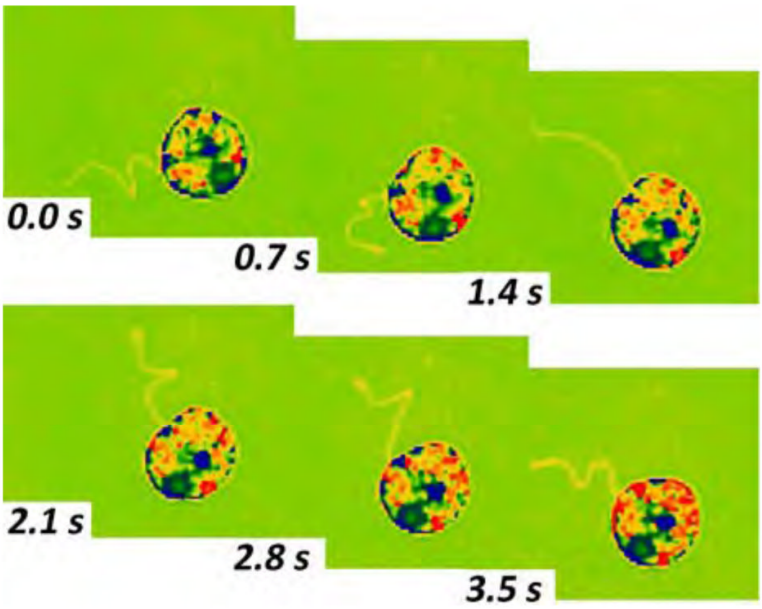

Fig. 4.
Flagellate with a body ~40 μm in diameter taken at 10X with a 660 nm source. Note detail of flagellar motion.

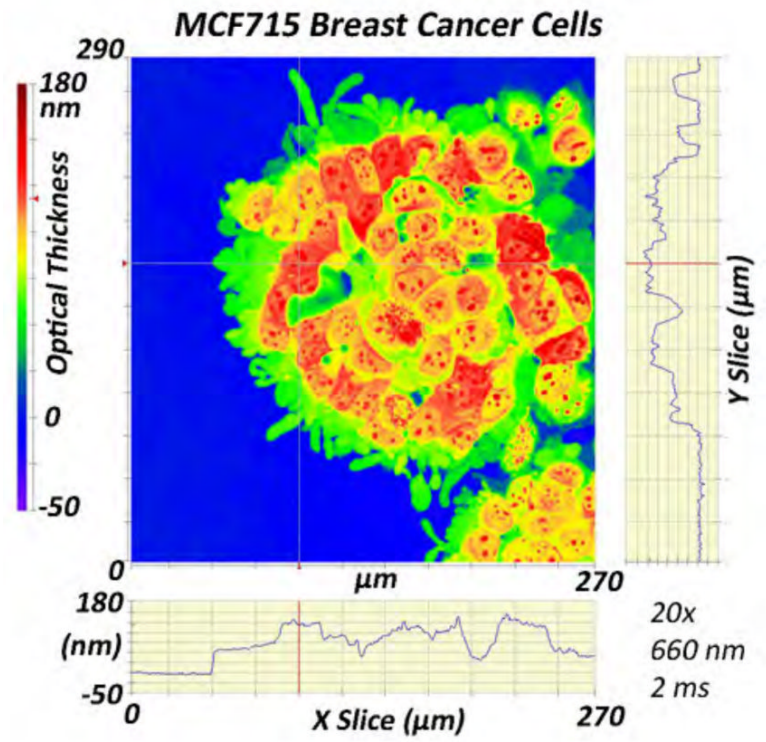

Fig. 5.
Culture of human breast cancer cell line grown on a coverslip taken at 20X with a 660 nm source.

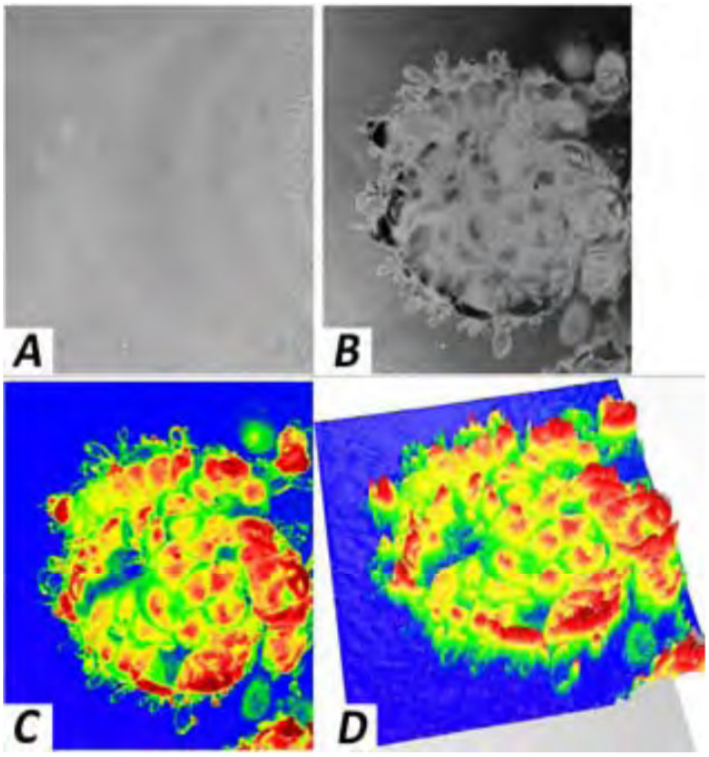

Fig. 6.

Human breast cancer cells of Fig. 5 after contact with purified water and then a KCL solution. (A) Brightfield image. (B) Interference image similar to phase contrast. (C) Phase image with pseudo-color representation of optical thickness scaled from −50 to 220 nm (a slightly larger scale than Fig. 5). Notice osmotic swelling of cells and shriveling of edge features compared to Fig. 5. (D) 3D plot of (C).

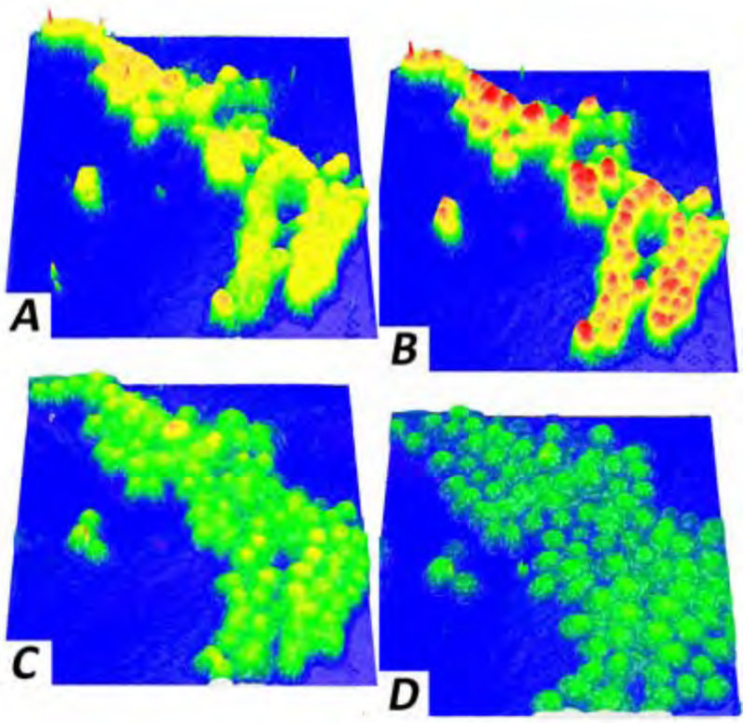

Fig. 7.

4D time series of 3D phase images of another breast cancer cell culture. All images have the same optical thickness pseudocolor scale from −100 to 450 nm. (A) Cells in original media. (B) After contact with purified water. (C) After more purified. (D) After contact with NaOH the cells are beginning to break down.

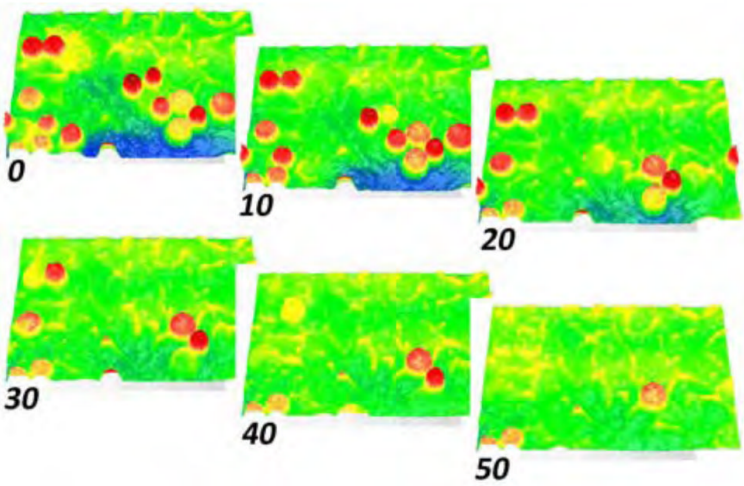

Fig. 8.

4D time series of phase images of breast cancer cells as they dissolve after contact with pure water, NaOH and Alconox®. Imaging area is 200 × 300 μm. Data are taken at 20X with a 660 nm source and 2 ms exposures. Samples above are every 10 seconds from a 78 second long movie. The P-V (peak-to-valley or maximum-to-minimum) is −120 to 120 nm.